This paper is published as part of a PCCP Themed Issue on:
Metal oxide nanostructures: synthesis, properties and applications

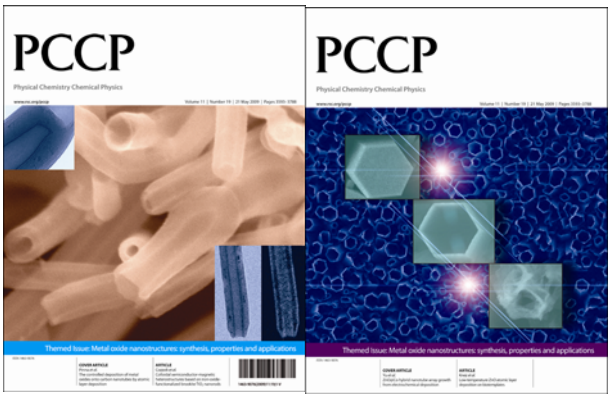

Guest Editors: Nicola Pinna, Markus Niederberger, John Martin Gregg and Jean-Francois Hochepied

Editorial

Chemistry and physics of metal oxide nanostructures
Phys. Chem. Chem. Phys., 2009
DOI: 10.1039/b905768d

Papers

Thermally stable ordered mesoporous CeO_2/TiO_2 visible-light photocatalysts
Guisheng Li, Dieqing Zhang and Jimmy C. Yu, *Phys. Chem. Chem. Phys.*, 2009
DOI: 10.1039/b819167k

Blue nano titania made in diffusion flames
Alexandra Teleki and Sotiris E. Pratsinis, *Phys. Chem. Chem. Phys.*, 2009
DOI: 10.1039/b821590a

Shape control of iron oxide nanoparticles
Alexey Shavel and Luis M. Liz-Marzán, *Phys. Chem. Chem. Phys.*, 2009
DOI: 10.1039/b822733k

Colloidal semiconductor/magnetic heterostructures based on iron-oxide-functionalized brookite TiO_2 nanorods
Raffaella Buonsanti, Etienne Snoeck, Cinzia Giannini, Fabia Gozzo, Mar Garcia-Hernandez, Miguel Angel Garcia, Roberto Cingolani and Pantaleo Davide Cozzoli, *Phys. Chem. Chem. Phys.*, 2009
DOI: 10.1039/b821964h

Low-temperature ZnO atomic layer deposition on biotemplates: flexible photocatalytic ZnO structures from eggshell membranes
Seung-Mo Lee, Gregor Grass, Gyeong-Man Kim, Christian Dresbach, Lianbing Zhang, Ulrich Gösele and Mato Knez, *Phys. Chem. Chem. Phys.*, 2009
DOI: 10.1039/b820436e

A LEEM/μ-LEED investigation of phase transformations in TiO_x/Pt(111) ultrathin films
Stefano Agnoli, T. Onur Menteş, Miguel A. Niño, Andrea Locatelli and Gaetano Granozzi, *Phys. Chem. Chem. Phys.*, 2009
DOI: 10.1039/b821339a

Synthesis and characterization of V_2O_3 nanorods
Alexander C. Santulli, Wenqian Xu, John B. Parise, Liusuo Wu, M.C. Aronson, Fen Zhang, Chang-Yong Nam, Charles T. Black, Amanda L. Tiano and Stanislaus S. Wong, *Phys. Chem. Chem. Phys.*, 2009
DOI: 10.1039/b822902c

Flame spray-pyrolyzed vanadium oxide nanoparticles for lithium battery cathodes
See-How Ng, Timothy J. Patey, Robert Büchel, Frank Krumeich, Jia-Zhao Wang, Hua-Kun Liu, Sotiris E. Pratsinis and Petr Novák, *Phys. Chem. Chem. Phys.*, 2009
DOI: 10.1039/b821389p

Mesoporous sandwiches: towards mesoporous multilayer films of crystalline metal oxides
Rainer Ostermann, Sébastien Sallard and Bernd M. Smarsly, *Phys. Chem. Chem. Phys.*, 2009
DOI: 10.1039/b820651c

Surprisingly high, bulk liquid-like mobility of silica-confined ionic liquids
Ronald Göbel, Peter Hesemann, Jens Weber, Eléonore Möller, Alwin Friedrich, Sabine Beuermann and Andreas Taubert, *Phys. Chem. Chem. Phys.*, 2009
DOI: 10.1039/b821833a

Fabrication of highly ordered, macroporous $Na_2W_4O_{13}$ arrays by spray pyrolysis using polystyrene colloidal crystals as templates
SunHyung Lee, Katsuya Teshima, Maki Fujisawa, Syuji Fujii, Morinobu Endo and Shuji Oishi, *Phys. Chem. Chem. Phys.*, 2009
DOI: 10.1039/b821209k

Nanoporous Ni–$Ce_{0.8}Gd_{0.2}O_{1.9-x}$ thin film cermet SOFC anodes prepared by pulsed laser deposition
Anna Infortuna, Ashley S. Harvey, Ulrich P. Muecke and Ludwig J. Gauckler, *Phys. Chem. Chem. Phys.*, 2009
DOI: 10.1039/b821473e

Surface chemistry of carbon-templated mesoporous aluminas
Thomas Onfroy, Wen-Cui Li, Ferdi Schüth and Helmut Knözinger, *Phys. Chem. Chem. Phys.*, 2009
DOI: 10.1039/b821505g

ZnO@Co hybrid nanotube arrays growth from electrochemical deposition: structural, optical, photocatalytic and magnetic properties
Li-Yuan Fan and Shu-Hong Yu, *Phys. Chem. Chem. Phys.*, 2009
DOI: 10.1039/b823379a

Electrochemistry of $LiMn_2O_4$ nanoparticles made by flame spray pyrolysis
T. J. Patey, R. Büchel, M. Nakayama and P. Novák, *Phys. Chem. Chem. Phys.*, 2009
DOI: 10.1039/b821572n

Ligand dynamics on the surface of zirconium oxo clusters
Philip Walther, Michael Puchberger, F. Rene Kogler, Karlheinz Schwarz and Ulrich Schubert, *Phys. Chem. Chem. Phys.*, 2009
DOI: 10.1039/b820731c

Thin-walled Er^{3+}:Y_2O_3 nanotubes showing up-converted fluorescence
Christoph Erk, Sofia Martin Caba, Holger Lange, Stefan Werner, Christian Thomsen, Martin Steinhart, Andreas Berger and Sabine Schlecht, *Phys. Chem. Chem. Phys.*, 2009
DOI: 10.1039/b821304f

Wettability conversion of colloidal TiO_2 nanocrystal thin films with UV-switchable hydrophilicity
Gianvito Caputo, Roberto Cingolani, Pantaleo Davide Cozzoli and Athanassia Athanassiou, *Phys. Chem. Chem. Phys.*, 2009
DOI: 10.1039/b823331d

Nucleation and growth of atomic layer deposition of HfO_2 gate dielectric layers on silicon oxide: a multiscale modelling investigation
A. Dkhissi, G. Mazaleyrat, A. Estève and M. Djafari Rouhani, *Phys. Chem. Chem. Phys.*, 2009
DOI: 10.1039/b821502b

Designing meso- and macropore architectures in hybrid organic–inorganic membranes by combining surfactant and breath figure templating (BFT)
Ozlem Sel, Christel Laberty-Robert, Thierry Azais and Clément Sanchez, *Phys. Chem. Chem. Phys.*, 2009
DOI: 10.1039/b821506e

The controlled deposition of metal oxides onto carbon nanotubes by atomic layer deposition: examples and a case study on the application of V_2O_4 coated nanotubes in gas sensing
Marc-Georg Willinger, Giovanni Neri, Anna Bonavita, Giuseppe Micali, Erwan Rauwel, Tobias Herntrich and Nicola Pinna, *Phys. Chem. Chem. Phys.*, 2009
DOI: 10.1039/b821555c

***In situ* investigation of molecular kinetics and particle formation of water-dispersible titania nanocrystals**
G. Garnweitner and C. Grote, *Phys. Chem. Chem. Phys.*, 2009
DOI: 10.1039/b821973g

Chemoresistive sensing of light alkanes with SnO_2 nanocrystals: a DFT-based insight
Mauro Epifani, J. Daniel Prades, Elisabetta Comini, Albert Cirera, Pietro Siciliano, Guido Faglia and Joan R. Morante, *Phys. Chem. Chem. Phys.*, 2009
DOI: 10.1039/b820665a

Ligand dynamics on the surface of zirconium oxo clusters†

Philip Walther,‡ Michael Puchberger, F. Rene Kogler, Karlheinz Schwarz* and Ulrich Schubert*

Received 20th November 2008, Accepted 2nd March 2009
First published as an Advance Article on the web 26th March 2009
DOI: 10.1039/b820731c

The dynamics of carboxylate ligands on the surface of zirconium oxo clusters was investigated in two case studies. Zr_4O_2(methacrylate)$_{12}$ was investigated by one- and two dimensional NMR spectra both in the solid state and in solution. In solution, the cluster is C_{2h} symmetric; stepwise intramolecular exchange of the four non-equivalent ligands was observed when the temperature was raised from −80 °C to −50 °C. The individual exchange processes were assigned to different ligand positions. *Ab initio* molecular dynamics simulations were performed for $Zr_6(OH)_4O_4$(formate)$_{12}$ to study the trajectory for the rearrangement of three chelating ligands into bridging positions, *i.e.* the conversion of the C_3-symmetric into an O_h-symmetric cluster. The observation of a dip in the energy barrier along the reaction coordinate was related to the intermediate formation of hydrogen bonds between the moving oxygen atom of the rearranging ligand and a μ_3-OH group of the cluster. Thus, the motion of the ligand requires a concerted motion in three dimensions.

1. Introduction

We have previously prepared a number of titanium and zirconium oxo clusters of various sizes and different carboxylate ligands for the preparation of cluster-crosslinked polymers.[1] Although the main goal was to use the clusters as nanosized building blocks for this new class of inorganic–organic hybrid materials, we also observed some interesting phenomena related to the chemistry of the clusters. For example, intermolecular carboxylate exchange between the cluster-bonded carboxylate ligands and free acid in solution was studied.[2,3] Furthermore, room temperature NMR spectra of many clusters exhibited averaged signals due to rapid intramolecular ligand exchange (''carboxylate shift''). Exchange processes between surface-bonded ligands and their environment as well as the dynamic site exchange of the ligands at the surface also play an important role for metal oxide nanoparticles, where carboxylate ligands are often used for the stabilization and functionalization of the nanoparticles.[4] Such processes are more easily investigated for clusters because of their molecular nature; clusters can thus be regarded as simple models for nanoparticles. A variable-temperature NMR study on the carboxylate shift in the tetranuclear clusters $Zn_4(OCCR)_6$(bdmap)$_2$ (R = Me or Et; bdmap = 1,3-bis(dimethylamino)-2-propanolate) has been reported in the literature.[5] The cluster consists of two pairs of zinc atoms, each bridged by two bridging (μ_2) and one bridging-chelating (η^2,μ_2) ligand; two pairs are connected by two bdmap ligands. Below 200 K, coalescence between the μ_2 and η^2,μ_2 ligands has been observed and a trajectory has been postulated involving rotation of the involved ligands.

In this paper we report on the dynamic intramolecular site exchange of the methacrylate ligands of $Zr_4O_2(OMc)_{12}$ (**1**) (OMc = methacrylate) as well as *ab initio* molecular dynamics simulation on a member of the $Zr_6(OH)_4O_4(OOCR)_{12}$ cluster type (**2**).

2. Results and discussion

NMR studies on the ligand dynamics of $Zr_4O_2(OMc)_{12}$

$Zr_4O_2(OMc)_{12}$ (**1**) is known to exist, in the solid state, in two isomeric forms, *viz.* a symmetric (**1sy**)[6] and an asymmetric form (**1as**)[7] (Fig. 1). The main difference between the two forms is that the asymmetric cluster **1as** contains one bridging-chelating (η^2,μ_2) methacrylate ligand that is converted to a ''normal'' μ_2-bridging ligand in **1sy**. The solution NMR spectra of **1as** and **1sy** are the same, *i.e.* the structures interconvert in solution. Therefore the differences are just due to different crystal environments. A third crystal structure is reported in this work (see ESI†): $Zr_4O_2(OMc)_{12}{\cdot}C_6H_6$ was obtained by crystallization of **1** from benzene. The crystal lattice contains benzene solvate molecules; however, the structural data and the geometry of the centrosymmetric cluster are nearly the same as that of (solvate-free) **1sy**.

We start the discussion of the structure of $Zr_4O_2(OMc)_{12}$ in solution with a closer look at the symmetry of the **1sy** form. Fig. 2 shows a schematic representation of the cluster viewed perpendicular to the plane of the four zirconium atoms. Two of the twelve methacrylate ligands are chelating and

Institute of Materials Chemistry, Vienna University of Technology, Getreidemarkt 9, A-1060, Wien.
E-mail: uschuber@mail.zserv.tuwien.ac.at, kschwarz@theochem.tuwien.ac.at

† Electronic supplementary information (ESI) available: Tables of crystallographic data, and selected bond angles and distances for $Zr_4O_2(OMc)_{12}{\cdot}C_6H_6$. CCDC reference number 710280. For ESI and crystallographic data in CIF or other electronic format see DOI: 10.1039/b820731c

‡ Present address: Faculty of Physics, University of Vienna, and Institute for Quantum Information and Quantum Optics, Austrian Academy of Sciences.

 This journal is © the Owner Societies 2009

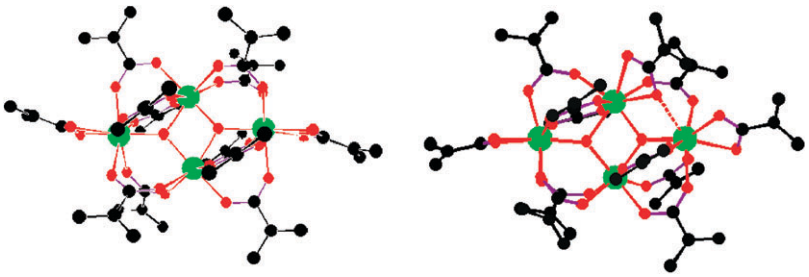

Fig. 1 Schematic structures of the two isomeric forms of the $Zr_4O_2(OMc)_{12}$ cluster. Left: symmetric $Zr_4O_2(OMc)_{12}$ (**1sy**); right: asymmetric $Zr_4O_2(OMc)_{12}$ (**1as**); the dashed line indicates the bridging character of one chelating methacrylate ligand.

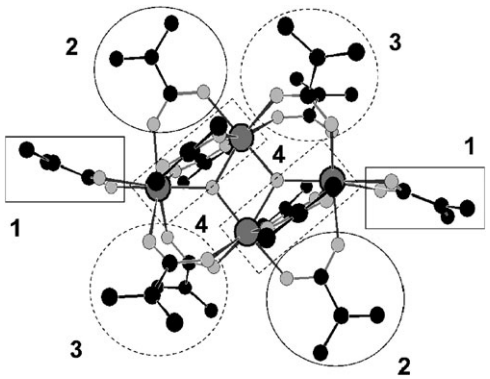

Fig. 2 Schematic presentation of the four non-equivalent ligand positions of the $Zr_4O_2(OMc)_{12}$ cluster (**1sy**). The different positions are marked with the numbers 1–4.

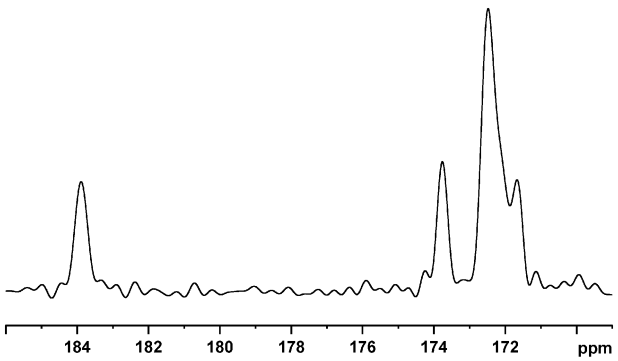

Fig. 3 Solid state ^{13}C-CP/MAS spectrum of $Zr_4O_2(OMc)_{12}$ (**1**), carbonyl-region.

coordinated to the zirconium at the terminal ends of the cluster (position 1). The remaining ten methacrylate ligands are bridging, two (position 2) being in the Zr_4 plane, four perpendicular to this plane (position 4) and four pairwise upwards and downwards orientated with an angle of 42.3° and 49.9° to the Zr_4 plane (position 3). The crystallographic symmetry of crystalline **1sy** is C_i. Neglecting the relative orientation of the methyl and methylene groups, the molecular symmetry of the cluster is C_{2h}. This leads to four non-equivalent ligand positions, *viz*. one chelating and three bridging positions and this should lead to four sets of signals in the NMR spectra with a signal ratio of 1:1:2:2. In Fig. 2, the ligands which give rise to a signal ratio of one in the NMR spectra are marked with full lines whereas the ligands which give raise to a signal intensity of 2 in the NMR spectra are marked with broken lines.

The ^{13}C-CP/MAS spectrum of $Zr_4O_2(OMc)_{12}$ (**1sy**) (Fig. 3) showed four well resolved signals in the carbonyl region, one of them bigger than the others and with a shoulder. Only one sharp set of methacrylate protons was observed at room temperature in CD_2Cl_2 solution. Temperature-dependent ^{1}H NMR spectra of the olefinic protons of $Zr_4O_2(OMc)_{12}$ (**1**) are shown in Fig. 4. The signals broadened by stepwise cooling of the solution. At −10 °C the two signals showed a broad coalescence and then split into multiple sets upon further cooling. At −80 °C eight sharp olefinic protons were observed, according to four different sets of ligands (bottom spectrum); the ratio of the four nonequivalent ligands was approximately 1:1:2:2, indicating the C_{2h} symmetry of the cluster in solution at this temperature.

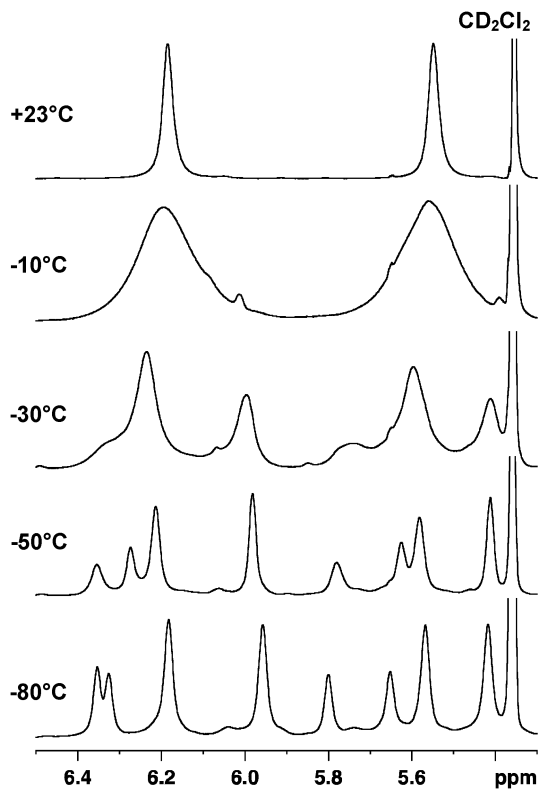

Fig. 4 Temperature-dependent ^{1}H NMR spectra of $Zr_4O_2(OMc)_{12}$ (**1**) in CD_2Cl_2 in the region of the olefinic protons.

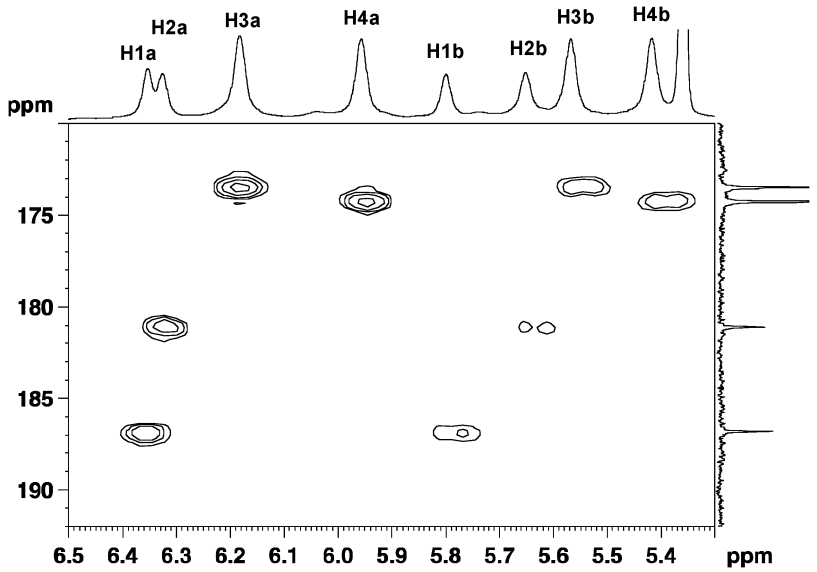

Fig. 5 $^{1}H/^{13}C$ HMBC spectrum of $Zr_4O_2(OMc)_{12}$ (**1**) in CD_2Cl_2 at −80 °C. Correlations between olefinic protons and carboxylate carbons are shown.

The signals can be partially assigned from the $^{1}H/^{13}C$ HMBC spectrum at −80 °C (Fig. 5). The two protons with chemical shifts of 6.34 (H1a) and 5.78 ppm (H1b), with the approximate intensity of one, gave long range correlations to the most downfield shifted carbonyl carbon at 186.8 ppm, that is thus assigned to a chelating carboxylate carbon (ligand position 1 in Fig. 2).[8] The signals of the other two protons which appeared with a relative signal intensity of one, H2a at 6.30 ppm and H2b at 5.65 ppm, gave correlations to 181.0 ppm; these signals were therefore assigned to a bridging carboxylate ligand, marked with a full circle and labeled "2" in Fig. 2. The four remaining proton signals appeared with a relative intensity of approximately two, *i.e.* H3a at 6.17 ppm and H3b at 5.56 ppm correlating to a carbonyl signal at 173.5 ppm and H4a at 5.95 ppm and H4b at 5.42 ppm correlating to a carbonyl signal at 174.2 ppm. These signals were assigned to the ligands which are marked with broken lines (number 3 and 4) in Fig. 2, but it is not possible to differentiate between them.

EXSY spectra at different temperatures were measured to learn more about the exchange mechanism (Fig. 6). The top left image shows the EXSY spectrum at −80 °C. The observed cross peaks are due to cross-correlation between neighboring olefinic protons of the methacrylate ligands, H1a–H1b, H2a–H2b, H3a–H3b, H4a–H4b and no exchange is detected. The situation changed at −70 °C, as shown in the second spectrum (Fig. 6 top right image). The cross correlation signal between H1a–H1b vanished whereas new signals appeared between H1a–H3a and H1b–H3b which are due to dynamic exchange. This means that the exchange with the lowest activation energy occurred between end-standing chelating ligands (Fig. 2, position 1) and one of the bridging ligands which are marked with broken lines (Fig. 2, ligand position 3 or 4). The movement of chelating ligands into a bridging position is possibly related to the observation of a bridging-chelating (η^2,μ_2) methacrylate ligand in **1as** or to the chelating-bridging transition described below for $Zr_6(OH)_4O_4(OOCR)_{12}$ clusters.

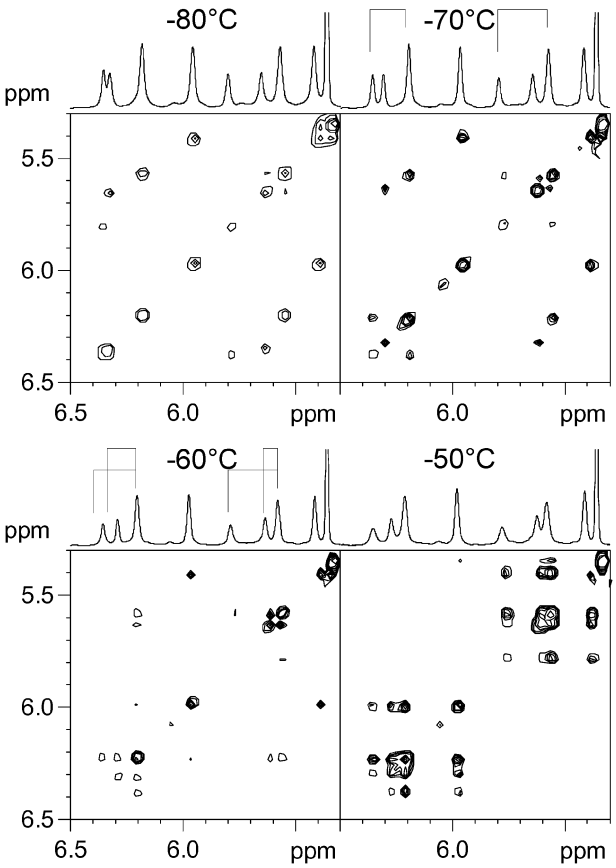

Fig. 6 EXSY spectra of $Zr_4O_2(OMc)_{12}$ (**1**) in CD_2Cl_2 with a mixing time of t_{mix} = 1 s at four different temperatures. Correlations of the olefinic protons are shown.

Up to −70 °C, the other two ligands were not involved in the exchange process. Upon raising the temperature to −60 °C, another ligand became involved in the exchange processes, shown in the bottom left image. Exchange signals were now

 This journal is © the Owner Societies 2009

observed between H1a–H2a–H3a and H1b–H2b–H3b whereas the fourth ligand is not involved in the exchange and still shows a cross correlation signal between the neighboring olefinic protons. Finally, the last spectrum measured at −50 °C (bottom right image) showed that all the ligands are now involved in the exchange processes. Exchange signals between H1a–H2a–H3a–H4a and H1b–H2b–H3b–H4b were detected and no cross-correlation peaks between these signals were left.

The stepwise exchange between the carboxylate ligands at low temperatures in solution is interesting and is in good agreement with the structure of the two isomeric forms of the crystalline cluster (Fig. 1). As can be seen, the change from a bridging to a chelating ligand position in the asymmetric cluster occurred at ligand position 3 (Fig. 2). The possible first exchange step could therefore occur between position 1 and position 3. The asymmetric form of the cluster could be the intermediate for the second exchange step observed in the EXSY spectrum at −60 °C (Fig. 6, bottom left) in which the ligand position 2 became involved in the exchange process. This assumption is confirmed by the fact that exchange peaks were observed between H3a–H1a, H3b–H1b and H3a–H2a, H3b–H2b but not between H1a–H2a, H1b–H2b, which means that position 1 is not involved in the exchange process between positions 2 and 3.

Ab initio molecular dynamics simulation of $Zr_6(OH)_4O_4(OOCH)_{12}$

A completely different way to learn about the dynamics of such systems is the use of molecular dynamics (MD) simulations, which, in the present case, were performed by means of an *ab initio* version based on density functional theory (DFT) described in the Experimental section.

The model system chosen for this study was a derivative of the cluster type $Zr_6(OH)_4O_4(OOCR)_{12}$ (**2**). X-ray structure analyses of three derivatives of **2** have been investigated, with RCOO = methacrylate (**2met**)[7] and *endo* or *exo* 5-norbornene-2-carboxylate (**2nor**).[9] The structure of **2** (Fig. 7, left) consists of a $Zr_6O_4(OH)_4$ core in which the triangular faces of a Zr_6 octahedron are alternatively capped by μ_3-O and μ_3-OH groups. Three carboxylate ligands chelate the zirconium atoms at one μ_3-O capped face (''chelated face''), while the other nine OOCR groups bridge all edges of the Zr_6 octahedron except the edges of the chelated face. Each zirconium atom is coordinated by eight oxygen atoms. The cluster core thus is C_{3v} symmetric with the C_3 axis passing through the center of the chelated face and the triangular face opposite to it, and the mirror planes bisecting these faces. In the ^{1}H and ^{13}C NMR data of **2met**, the signals in the room temperature spectra can be clearly assigned to three non-equivalent ligand positions (one chelating and two different bridging positions) according to the C_{3v} symmetry of the cluster in the crystalline state.[2]

The cluster type **2** rather than **1** was chosen for the DFT calculations for the following reasons: (ii) The NMR studies of **1** had shown that conversion of a chelating to a bridging coordination is the process with the lowest activation energy. Since clusters **2** also have chelating carboxylate ligands (in their crystal structures), we anticipated that DFT calculations would elucidate the trajectory of this process. (ii) At least three different exchange processes are responsible for the dynamics of the ligands in **1**. Using a cluster with a higher symmetry and thus fewer possibilities for ligand exchange should facilitate the DFT calculations. (iii) On the other hand, dynamic NMR investigations of the clusters **2** were partially ambiguous due to the high tendency of these clusters for hydrogen-bonding. Theoretical simulations on isolated clusters would thus provide a picture undisturbed by any interaction of the clusters with their environment.

A derivative of the cluster **2** with smaller ligands but the same cluster core as described above, *i.e.* the formate derivative $Zr_6(OH)_4O_4(OOCH)_{12}$ (**2for**), was used for the calculations. This is justified from a chemical point of view because this change should have no or only a marginal influence on the overall dynamic behavior of the ligands.

As a first step we put structure **2for** into a sufficiently large unit cell to avoid interactions with the periodic images which occur due to the periodic boundary conditions. All atoms should reach their equilibrium positions, *i.e.* no forces act on them and the corresponding total energy has a minimum. In general, all structures were relaxed without any constraints or symmetry requirements but the initial configuration of the ligands was predefined by the experimental data (see below) and thus the structure optimization found the nearest local (rather than the global) minimum of the potential hypersurface. Test calculations demonstrated that **2for** has the same low temperature structure as the methacrylate-substituted cluster **2met** (see Fig. 7, left). Therefore the structural simplification, which reduces the necessary computer time, is justified. A finite temperature molecular dynamics simulation showed that this structure is stable. This finding was further supported by a HOMO-LUMO gap of 4.062 eV.

From the structure optimization of **2for** we found that the zirconium atoms form an almost ideal octahedron (with Zr–Zr distances of 355.4, 357.2 and 359.7 pm). In the following, the Zr atoms forming the ''chelated face'' of the octahedron are labeled ''Zr(1)'' while the Zr atoms of the opposite face are labeled ''Zr(2)''. The different types of O- or OH-capped Zr_3 triangles and the labeling of the capping oxygen atoms are shown in Fig. 8. Carboxylate ligands bridging Zr(l) and one Zr(2) atom are labeled L(12), those bridging two Zr(2) atoms L(22) and the chelating ligands L(11). The 3-fold axis passes through the centers of these faces and the two oxygen atoms O(111) (μ_3-O) and O(222) (μ_3-OH). The two other oxygens, *viz.* O(112) and O(122), are capping the remaining six faces of the octahedron. The μ_3-oxygen O(122) is located above a Zr(l), Zr(2), Zr(2) face with the distances Zr(l)–O(122) of 208.1 pm and Zr(2)–O(122) of 208.6 pm. In contrast, the μ_3-OH oxygen O(112) is asymmetrically bonded with two short bonds (226.0 pm) to the Zr(l) atoms, and a very long bond to Zr(2) (242.9 pm). The possible origin of the different bond lengths and the asymmetry of the μ_3-OH group have been previously discussed.[7]

Table 1 compares (calculated) distances of **2for** with experimental X-ray data of **2met**. The largest difference was obtained for the distance Zr(2)–L(22) of 14.7 pm (6%). Note that the standard deviation for the experimental Zr–O bonds is relatively high.

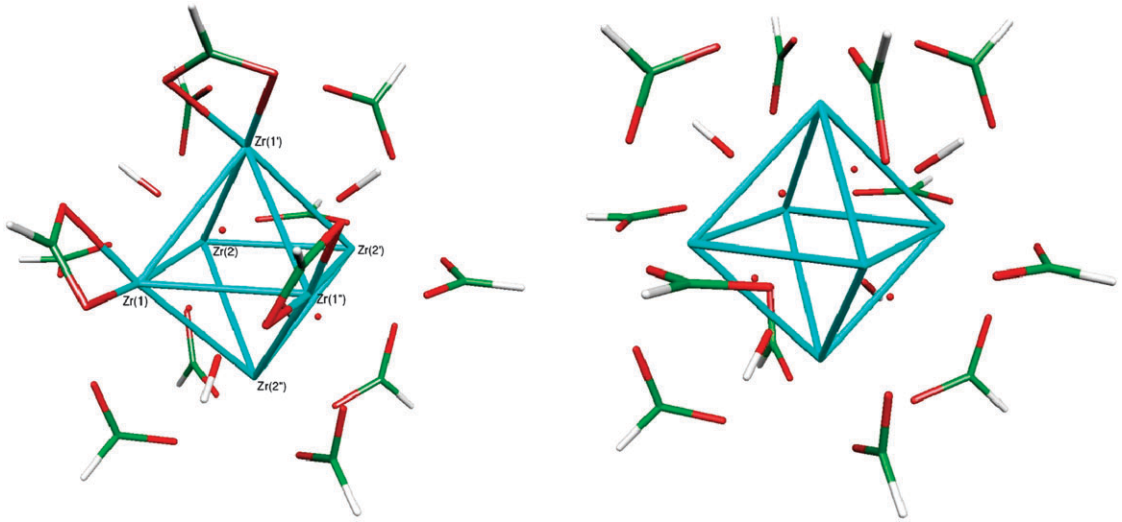

Fig. 7 Structure of the calculated structures of the cluster **2for**. There are no bonds between the zirconium atoms; the lines just serve for visualizing the zirconium cluster core. All ligands are bonded to the zirconium atoms, but only the Zr–O bonds at the chelated face are shown for simplicity. Left: C_3-symmetric cluster; right: O_h-symmetric cluster (see text).

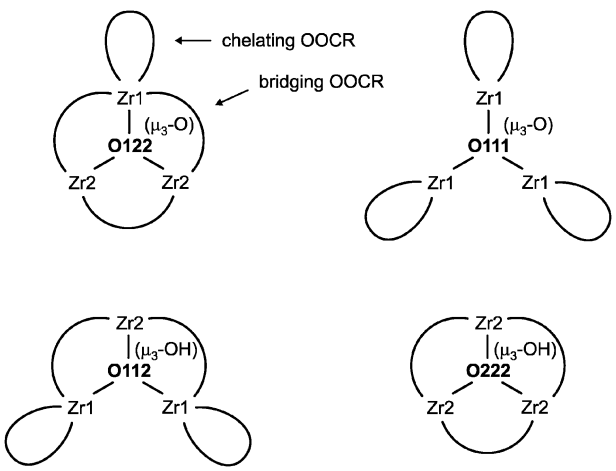

Fig. 8 The different types of O- or OH-capped Zr triangles of the C_3-symmetric cluster **2**.

Table 1 Comparison of selected bond lengths [pm] of the formate-substituted cluster **2for** (calculated) and the methacrylate-substituted cluster **2met** (solid-state structure) (L = oxygen atoms of the ligands)

		Distance A–B [pm]	
A	B	Theory (**2for**)	Expt. (**2met**)
	Zr(1)	359.7	350.6 (4)
	Zr(2)	355.4	348.0 (2)
Zr(1)	L(11)	228.9	233 (2)
	L(12)	225.9	219 (2)
	μ_3-O(111)	213.2	209.5 (5)
	μ_3-O(122)	208.1	206 (1)
	μ_3-O(112)H	226.0	217 (1)
	Zr(2)	357.2	354.8 (4)
Zr(2)	L(22)	224.7	210 (1)
	L(12)	222.4	213 (1)
	μ_3-O(222)H	230.0	229 (1)
	μ_3-O(122)	208.1	205.0 (7)
	μ_3-O(112)H	242.9	241 (2)

The crystallographically observed structures for the clusters **2** were somewhat surprising. From simple structural considerations one would rather expect an octahedral symmetry with exclusively edge-bridging ligands for an octahedral cluster with 8 face-capping and 12 bidentate ligands. In order to investigate the differences in bonding between bridging and chelating ligands, a model system with only bridging ligands was also studied (Fig. 7, left).

The total energy of this O_h-symmetric cluster was lower by 16.81 mH (44.13 kJ) than that of the C_3-symmetric cluster with three chelating ligands (Fig. 7, right). The six zirconium atoms in this high-symmetry model cluster form a perfect octahedron (Zr–Zr distance 356.6 pm). The triangular faces are occupied alternately by μ_3-O and μ_3-OH groups. The μ_3-O groups have shorter Zr–O distances (209.1 pm) than the μ_3-OH groups (228.8 pm). All Zr–O distances of the bridging formate ligands are the same by symmetry, *viz*. 225.8 pm.

The lower energy of the O_h-symmetric cluster is in contrast to the experimentally observed stability of the C_3-symmetric clusters both in the crystalline state[7,9] and in solution.[3] However, the crystal structures of this cluster type are characterized by extensive hydrogen bonds to co-crystallizing carboxylic acids (clusters act both as hydrogen donors [OH groups] and hydrogen acceptors), which are excluded in the theoretical model. As a matter of fact, clusters of this type have not yet been crystallized without hydrogen-bonded carboxylic acids. The same may be true in solution, where additional carboxylic acids, solvent effects or inter-cluster hydrogen bonds cannot be excluded. In the theoretical simulations, however, only isolated clusters were treated.

The fact that both the C_3 and O_h-symmetric cluster **2for** were accessible by quantum mechanical calculations, allowed MD simulations to study the conversion between the two forms. An MD simulation of the cluster at 700 K for 3 ps showed mainly rotational excitations, but no change in the main bonding characteristics. In order to study the latter we had to use constraints, *i.e*. we carried out simulations, in which

 This journal is © the Owner Societies 2009

we forced the ligands to move from a chelating to a bridging position. For computational reasons we assumed that the ligands move in a synchronized way, which approximately can be expected to occur in reality because of the absence of steric interactions. A constraint was used to force one oxygen atom of a chelating ligand to move from Zr(l) to a neighboring Zr(1′) in a synchronized fashion, *i.e.* for all three equivalent Zr(1) atoms. Bonding of the second oxygen of the chelating formate to Zr(1) was retained during the movement. This corresponds to a motion, where one changes the ligand arrangement shown in the right row of Fig. 8 from top to bottom by simultaneously moving three oxygen atoms (one from each chelating formate ligand) from one Zr(1) atom to the neighboring one. In the MD calculation the stepwise motion of the oxygen atoms from one Zr atom to the neighboring Zr atom was forced, but the O atom was allowed to move freely perpendicular to the reaction coordinate (sometimes this is called the umbrella method). A direct MD simulation could find this motion too, but it would require much longer simulation times. The chosen procedure allowed scanning the energy surface, when the oxygen atoms change from chelating to bridging positions (Fig. 9). The energy is low at the chelating and bridging configurations (*i.e.* at the start and the end of the forced movement). However, there is a pronounced minimum in between, which is due to an interaction with a μ_3-OH group. Note that the [Zr(1)/Zr(1)/Zr(1)] plane (top right in Fig. 8) is surrounded by three [Zr(1)/Zr(1)/Zr(2)] faces with capping μ_3-OH groups (bottom left in Fig. 8). The energy minimum also corresponds to the shortest distance between the oxygen of the moving ligand and the hydrogen of the μ_3-OH group.

The observation of a dip in the energy barrier (Fig. 9, left scale) along the reaction coordinate appears to be a more general feature of such systems. It comes about by forming hydrogen bonds between the moving ligand and neighboring OH groups (Fig. 9, right scale). Thus, the motion of the ligand cannot be understood by changing just one parameter, but instead requires a concerted motion in three dimensions.

3. Experimental

NMR investigation of 1

Cluster **1** was prepared and crystallized as previously described.[6,7] To remove solvate molecules from the crystalline cluster, the compound was dissolved in water-free CH_2Cl_2 and all volatiles were removed *in vacuo*. This procedure was repeated several times and finally the solid residue was dried at room temperature at 10^{-5} mbar for several hours. All solution NMR spectra were recorded on a Bruker *Avance* 300 (^{1}H at 300.13 MHz, ^{13}C at 75.13 MHz) equipped with a 5 mm inverse broadband probe head with z-gradient unit. 2D spectra were measured with Bruker standard pulse sequences: COSY (Correlated Spectroscopy), HSQC (Heteronuclear Single Quantum Correlation), HMBC (Heteronuclear Multiple Bond Correlation), EXSY (Exchange Spectroscopy), NOESY (Nuclear Overhauser Effect Spectroscopy), ROESY (Rotating Frame Overhauser Effect Spectroscopy). Gas-tight Young tubes were used for all experiments. CD_2Cl_2 was purchased from Euriso-Top (99.8%). The solid state spectrum was measured on a Bruker *Avance* 300 (at 299.85 MHz ^{13}C at 75.4 MHz) equipped with a 4 mm broadband probe-head. CP/MAS spectra were measured at a rotor frequency of 8 kHz.

Molecular dynamics simulations

All molecular dynamics simulations were carried out with the Car-Parrinello Projector Augmented Wave (CP-PAW) code developed by Blöchl.[10] The wave function is expanded in plane waves up to an energy cut-off of 30 Ryd. The frozen-core approximation was applied for shells below the 4s electrons of Zr and for the 1s electrons of O and C. Core data were imported from scalar relativistic atomic calculations. All

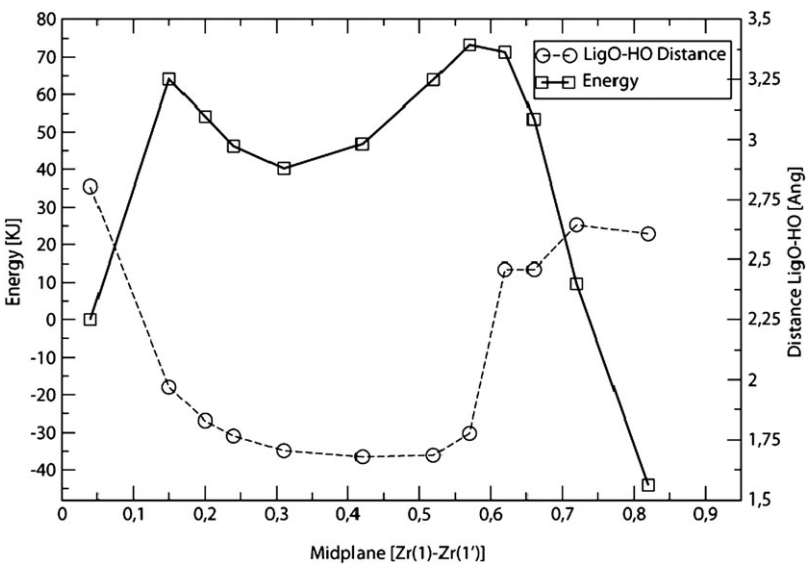

Fig. 9 Energy profile (left scale) for the ligands movement (synchronized) from chelating (left) to bridging positions (right). The corresponding "reaction coordinate" is given by the midplane value from 0 to 1, where 0 corresponds to the original chelating Zr(1) and 1 to the neighboring Zr(1′). The distance between the moved carboxylate oxygen and the hydrogen of the μ_3-OH group is given on the right scale.

simulations were performed using the local density approximation in the parameterization of Perdew and Wang,[11] with the generalized gradient approximation (GGA) by Perdew, Burke and Ernzerhof.[12] We used periodic boundary conditions with a 24 nm primitive cell, which was found to be sufficiently large to prevent wave function overlaps between neighboring images. Long-range electrostatic interactions between different cells are eliminated using a method by Blöchl, which is based on fitting an atom-centered Gaussian charge density to the molecular electronic density. A time step of 10 au was used to integrate the equation of motion, correcting the mass of the nuclei to account for the drag of the electrons[13] in the coupled dynamics integrated with the Verlet algorithm.[14] The temperature of the nuclei was controlled by a Nose thermostat,[15] which creates a canonical (NVT) ensemble. To sample phase space in the vicinity of the transition state, a reaction coordinate (RC) was chosen which was kept constrained during the dynamics using SHAKE constraints.[16] All other degrees of freedom were allowed to evolve naturally in time. By slowly varying the constraint, phase space in the vicinity of the transition state can be sampled dynamically, leading to undisturbed dynamics for all motions which are orthogonal to the RC, and to fictitious dynamics along the RC. This renders possible to investigate even high-lying transition states, such as those encountered in the present study.

4. Conclusions

In this paper we have investigated the dynamic intramolecular exchange of carboxylate ligands on the surface of two zirconium oxide clusters by two complementary methods, *viz*. dynamic NMR spectroscopy and molecular dynamics simulations. Metal oxide clusters of the early transition metals are particularly well suited for studying ligand dynamics, because these are stable in solution and diamagnetic. However, the findings presented in this article are not restricted to the zirconia clusters studied here, but should be valid both for carboxylate-substituted clusters of other transition metals as well as nanoparticles. Carboxylate ligands are often used for the stabilization and functionalization of nanoparticles. It is reasonable to assume that dynamic site exchange of ligands, as described in this article, also occur on the surface of nanoparticles. Clusters can thus be regarded as simple models for nanoparticles where such processes are more easily investigated for clusters because of their molecular nature.

Despite the different chemical composition, the clusters **1** and **2** have in common that they contain both bridging and chelating carboxylate ligands. Clusters of type **2** are additionally characterized by the presence of μ_3-OH groups in addition to μ_3-O groups.

An initial important result of this study is that an octahedral geometry of **2for**, in which all ligands occupy bridging positions, would be more stable than the experimentally observed C_3-symmetric geometry with three chelating ligands. Thus, solvent effects and the H-bonded carboxylic acids present in all crystal structures of derivatives of **2** must be responsible for the observed geometry in the crystalline state and in solution.

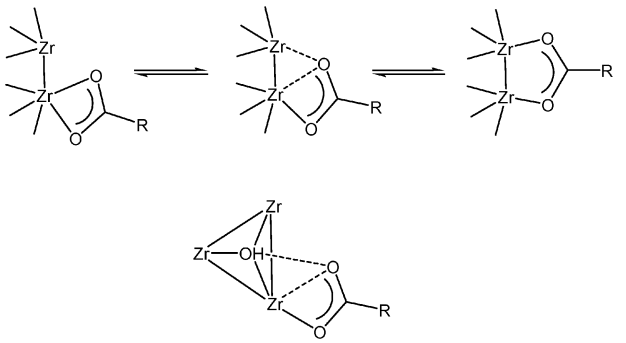

Fig. 10 Proposed trajectories for the chelating-bridging rearrangement of carboxylate ligands in **1** and **2**.

A second conclusion is that a chelating-bridging rearrangement of carboxylate ligands is a very favorable process that probably accounts to a large extent for the dynamics of the ligand shell. In the case of $Zr_4O_2(OMc)_{12}$ (**1**) the ligand exchange process with the lowest activation energy involves the chelating ligands that dynamically exchange positions with one kind of bridging ligands already above -70 °C. In **2for**, the simultaneous rearrangement of the three chelating ligands in a bridging coordination mode is a facile process with an activation barrier of $+73.3$ kJ/mol.

Comparison of the structures of **1as** and **1sy** indicates that the chelating–bridging transition (and return) occurs *via* a bridging–chelating (η^2,μ_2) coordination as found for one methacrylate ligand in **1as** (upper part of Fig. 10). In the case of **2for**, the theoretical calculations show that this coordination mode is preceded by a hydrogen bond between the moving oxygen atom of the carboxylate and an adjacent OH-group. When calculating the energy surface for the chelating-bridging transition of the ligands in **2**, an energy barrier of $+64.1$ kJ is first observed, but the system then reaches a metastable state ($+40.2$ kJ). This stabilization of the ligand O-atoms is due to hydrogen bonds to the μ_3-OH groups (lower part of Fig. 10). Finally the energy increases again over a barrier ($+73.3$ kJ) during which the hydrogen bonds break and the carboxylate ligand enters a bridging coordination.

Acknowledgements

This work was supported by the Fonds zur Förderung der wissenschaftlichen Forschung (FWF), Austria.

References

1 Review articles: U. Schubert, *Chem. Mater*., 2001, **13**, 3487; G. Kickelbick and U. Schubert, *Monatsh. Chem*., 2001, **132**, 13.
2 F. R. Kogler, M. Jupa, M. Puchberger and U. Schubert, *J. Mater. Chem*., 2004, **14**, 3133.
3 M. Puchberger, F. R. Kogler, M. Jupa, S. Gross, H. Fric, G. Kickelbick and U. Schubert, *Eur. J. Inorg. Chem*., 2006, 3283.
4 Review article: M.-A. Neouze and U. Schubert, *Monatsh. Chem*., 2008, **139**, 183.
5 A. Demšar, J. Košmrij and S. Petriček, *J. Am. Chem. Soc*., 2002, **124**, 3951.
6 G. Trimmel, S. Gross, G. Kickelbick and U. Schubert, *Appl. Organomet. Chem*., 2001, **15**, 401.
7 G. Kickelbick and U. Schubert, *Chem. Ber*., 1997, **130**, 473.
8 B.-H. Ye, X.-Y. Li, I. D. William and X.-M. Chen, *Inorg. Chem*., 2002, **41**, 6426.

 This journal is © the Owner Societies 2009

9 Y. Gao, F. R. Kogler, H. Peterlik and U. Schubert, *J. Mater. Chem.*, 2006, **16**, 3268.
10 P. E. Blöchl, *Phys. Ref. B*, 1994, **50**, 17953.
11 J. P. Perdew and Y. Wang, *Phys. Rev. B*, 1992, **45**, 13244.
12 J. P. Perdew, K. Burke and M. Ernzerhof, *Phys. Rev. Lett.*, 1996, **77**, 3865.
13 P. Blöchl and M. Parrinello, *Phys. Rev. B*, 1992, **45**, 9413.
14 L. Verlet, *Phys. Rev.*, 1967, **159**, 98.
15 S. Nose, *Mol. Phys.*, 1984, **52**, 255.
16 J.-P. Ryckaert, G. Ciccotti and H. J. Berendsen, *J. Comp. Phys.*, 1977, **23**, 327.